https://doi.org/10.5194/acp-2020-1027
Preprint. Discussion started: 28 October 2020

Atmospheric Chemistry and Physics
Open Access
Discussions

Carbonaceous aerosol composition in air masses influenced by large-scale biomass burning: a case-study in Northwestern Vietnam

Dac-Loc Nguyen[1,2,8], Hendryk Czech[1,2], Simone M. Pieber[3], Jürgen Schnelle-Kreis[1], Martin Steinbacher[3], Jürgen Orasche[1], Stephan Henne[3], Olga B. Popovicheva[4], Gülcin Abbaszade[1], Günter Engling[5,a], Nicolas Bukowiecki[6], Nhat-Anh Nguyen[7], Xuan-Anh Nguyen[8], Ralf Zimmermann[1,2]

[1]Joint Mass Spectrometry Centre (JMSC), Cooperation Group "Comprehensive Molecular Analytics" (CMA), Helmholtz Zentrum München, München, 81379, Germany
[2]Joint Mass Spectrometry Centre (JMSC), Chair of Analytical Chemistry, University of Rostock, Rostock, 18059, Germany
[3]Empa, Laboratory for Air Pollution/Environmental Technology, Dübendorf, Switzerland
[4]Skobeltsyn Institute of Nuclear Physics, Moscow State University, Moscow, 119991, Russian Federation
[5]Department of Biomedical Engineering and Environmental Sciences, National Tsing Hua University, Hsinchu 30013, Taiwan
[6]Department of Environmental Sciences, University of Basel, Basel, 4056, Switzerland
[7]Hydro-Meteorological Observation Center, Vietnam Meteorological and Hydrological Administration, Ministry of Natural Resources and Environment, Ha Noi, Vietnam
[8]Institute of Geophysics, Vietnam Academy of Science and Technology (VAST), Ha Noi, Vietnam
[a]now at: Mobile Source Laboratory Division, California Air Resource Board, El Monte, CA 91731, United States

Correspondence to: Hendryk Czech (hendryk.czech@uni-rostock.de; hendryk.czech@helmholtz-muenchen.de)

Abstract. We investigated concentrations of organic carbon (OC), elemental carbon (EC) and a wide range of particle-bound organic compounds in daily sampled $PM_{2.5}$ at the remote Pha Din (PDI) - Global Atmosphere Watch (GAW) monitoring station in Northwestern Vietnam during an intense 3-week sampling campaign from 23rd March to 12th April 2015. The site is known to receive trans-regional air masses during large-scale biomass burning episodes, but OC composition studies are missing in the scientific literature. We quantified 51 organic compounds simultaneously by in-situ derivatization thermal desorption gas chromatography time-of-flight mass spectrometry (IDTD-GC-TOFMS). Anhydrosugars, methoxyphenols, n-alkanes, fatty acids, polycyclic aromatic hydrocarbons, oxygenated polycyclic aromatic hydrocarbons, nitrophenols as well as OC were used in a hierarchical cluster analysis highlighting distinctive patterns for periods under low, medium and high biomass burning (BB) influence. The highest particle phase concentration of the typical primary organic aerosol (POA) and possible secondary organic aerosol (SOA) constituents, especially nitrophenols, were found on 5th and 6th April. We linked the trace gases CH_4, CO_2, CO, O_3 mixing ratios to the statistical classification of BB events based on OA composition and found increased CO and O_3 levels during medium and high BB influence. Likewise, a backward trajectory analysis indicates different source regions for the identified periods based on the OA cluster, with cleaner air masses arriving from northeast, i.e., mainland China and Yellow sea. The more polluted periods are characterized by trajectories from southwest, with more continental recirculation of the medium cluster, and more westerly advection for the high cluster. These findings highlight that BB activities in Northern Southeast Asia cannot only significantly enhance the regional organic aerosol loading, but also affect the carbonaceous $PM_{2.5}$ constituents and the trace gases in northwestern Vietnam. The presented analysis adds valuable data on the carbonaceous and in particular OC chemical composition of $PM_{2.5}$ in a region of scarce data availability.

1 Introduction

The Northern Southeast Asia region is well known for emission-intense and recurring wildfires and after-harvest crop residue burning during the pre-monsoon season from February to April. Atmospheric aerosol concentrations and haze events typically peak during these periods and have found previously to be correlated with biomass burning (BB) activity, which contribute considerably to the regional aerosol loadings (Streets et al., 2003;Carmichael et al., 2003;Gautam et al., 2013;Lee et al., 2016). Open BB plumes from e.g., wildfires or agricultural burning can be transported over long distances along with the prevailing westerly winds and may also influence the large-scale atmospheric circulation in Northern Southeast Asia (Lin et al., 2013;Reid et al., 2013;Tsay et al., 2016). The widespread occurrence of episodic open BB emission in Southeast Asia results in the "river of smoke aerosols" from near source regions over northern Thailand-Laos-Vietnam and depicts the confluence of aerosol-cloud-radiation interactions prior to entering the receptor areas of Hong Kong, southeastern Tibetan Plateau or central Taiwan (Lin et al., 2013;Yen et al., 2013;Chan, 2003;Engling et al., 2011;Nguyen et al., 2016;Lee et al., 2016).

Open BB emits substantial amount of carbon monoxide (CO), several volatile organic compounds and primary organic aerosol (POA). During atmospheric transportation, smoke plumes may undergo complex physical, photochemical and multiphase reaction processes, which is known as "atmospheric aging". It generates secondary organic aerosol by oxidative conversion of organic vapors into the particle phase or aged POA by heterogeneous reaction between gas phase oxidants and POA or homogeneous reaction within the liquid phase of a particle (Seinfeld and Pandis, 2016). Consequently, atmospheric aging affects the light absorbing properties of the aerosol particles (Martinsson et al., 2015;Zhong and Jang, 2014) as well as adverse health effects of the smoke (Kanashova et al., 2018;Ihantola et al., 2020;Pardo et al., 2020) may change (Nordin et al., 2015;Gilmour et al., 2015). Detailed chemical analysis of the highly complex OC fraction of ambient PM samples collected downwind of BB as well laboratory-generated BBOA and aging in oxidation reactors (Bruns et al., 2015;Ihalainen et al., 2019) combined with *in vitro* and *in vivo* exposures may provide insights into potentially harmful constituents, atmospheric transformation processes and optical aerosol properties through marker compounds representative of POA and SOA.

The Pha Din Global Atmosphere Watch (GAW) regional monitoring station, PDI, is located in the north of the Indochina Peninsula, where there are BB activities during pre-monsoon season from February to April (Lin et al., 2013). Continuous observations of aerosol optical properties and greenhouse gases have been implemented at PDI since early 2014, and aerosol optical properties have been previously discussed by Bukowiecki et al. (2019). However, the source apportionment was only based on light-absorbing carbon and levoglucosan concentrations. So far, very few studies (Nguyen et al., 2016;Popovicheva et al., 2016;Popovicheva et al., 2017;Pham et al., 2019) investigated the organic chemical composition of aerosol samples collected in Northwestern Vietnam during BB events in detail. We complement the analysis by Bukowiecki et al. (2019) and present results from the chemical analysis of $PM_{2.5}$ samples and trace gas measurements collected during the BB season in 2015 at PDI. We discuss the daily variations of bulk carbonaceous components (OC, EC), and provide a detailed chemical analysis of organic aerosol constituents, including anhydrous sugars, methoxyphenols, n-alkanes, fatty acids, PAHs, o-PAHs, and nitro-phenols and add valuable data to the available body of literature. We deploy a hierarchical clustering approach to the OA constituents for source and process identification, and complement this analysis with interpretation of hourly trace gas data (CH_4, CO_2, CO, O_3) and backward trajectory analysis.

2 Methods

2.1 Site description

Data were collected at the PDI site (1466 m a.s.l., 21.573°N 103.516°E), a meteorological station of the Vietnam Meteorological and Hydrological Administration (VNMHA) and a regional station of the World Meteorological Organization's (WMO) Global Atmosphere Watch (GAW) program since 2014. Aside of instrumentation to collect meteorological data, the site is equipped with continuous in-situ observations of aerosol optical properties and trace gases, as described in Bukowiecki et al. (2019). The station is located in Dien Bien Province, which is 360 km northwest of Hanoi, 200 km south of the border with China, and 120 km east of the border with Laos (Figure 1). The province covers a vast area of 9541 km², and the population is estimated to be approximately 567'000 inhabitants as of 2017 (http://www.gso.gov.vn/). The observation site is located on the top of a hill about 1 km north of the Pha Din pass. There, the national highway AH13 runs connecting Son-La city (to the southeast) and Dien-Bien-Phu city (to the west). Within 5 km from the sampling site, there are only a few ethnic H'mong households using wood log and debris for residential cooking and heating. There are no industrial facilities in vicinity of the station.

2.2 Sampling campaign

An intense sampling campaign was conducted from 23rd March to 12th April in 2015 to complement continuous on-line monitoring with more detailed information on the aerosol particle composition. $PM_{2.5}$ (fine inhalable particles) samples were collected on 47 mm quartz-fiber filters (Whatman QM/A, Piscataway, NJ, USA) by MiniVol™ TAS (Airmetric, Eugene, OR, USA) samplers (sampling height of 2 m) with an operating flow rate at 5 L min^{-1} in the meteorological garden. The sampling duration was 24 hours, starting from 8:00 a.m. local time (UTC+7), and a total of 20 filters were collected. Sampling was conducted continuously, except for 25th March, when a filter had to be discarded due to a battery failure.

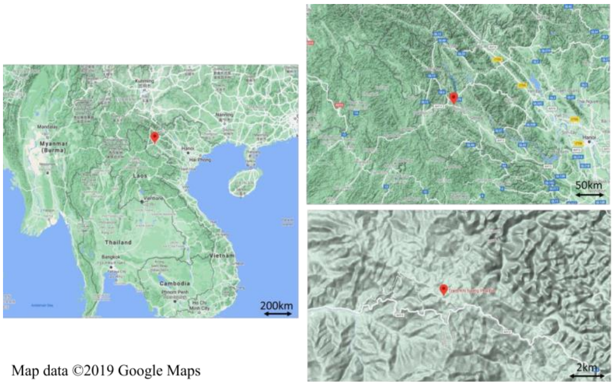

Map data ©2019 Google Maps

Figure 1. Maps showing PDI monitoring station, Dien-Bien Province, Vietnam, in three different scales of 200 km, 50 km, and 2 km. The maps are retrieved from the Google Terrain Map product.

2.3 Analysis of organic $PM_{2.5}$ composition

Bulk analysis of organic $PM_{2.5}$ constituents was performed with a thermal-optical carbon analyzer (DRI model 2001A) for the determination of Organic Carbon (OC) and Elemental Carbon (EC) following the Improve A protocol (Chow et al., 2004a) defining four fractions of OC (OC1-OC4) and three fractions of EC (EC1-EC3). Pyrolytic OC (OP) from caused by char formation was subtracted from apparent EC1 by using the filter reflectance via a He-Ne laser at 632.8 nm.

The measurement uncertainty δy was calculated as following Equation (1):

$$\delta y = [(\text{analyte concentration} \cdot \text{instrument precision})^2 + \text{LOD}^2]^{1/2} \qquad (1)$$

with LOD being the limit of detection.

For targeted chemical analysis, the in-situ derivatization thermal desorption - gas chromatography time-of-flight mass spectrometry (IDTD-GC-TOFMS) with electron ionization (EI) was used (Orasche et al., 2011). In order to avoid thermal decomposition of analytes and lowering limits of detection, hydroxyl and carboxyl groups of compounds, for example of anhydrosugars, were derivatized by N-Methyl-N-trimethylsilyltrifluoroacetamide (MSTFA) during the step of thermal desorption from quartz fiber filter in glass-goose-neck liner at 300°C. Detected compounds were identified by library match of EI mass spectra as well as retention index and quantified by isotope-labelled internal standards of the same substance or chemically similar substance. In total, 51 particle-bound organic compounds were quantified, covering the substance classes of polycyclic aromatic hydrocarbons (PAHs), oxygenated PAHs (o-PAHs), n-alkanes, anhydrosugars, fatty acids (carboxylic acids with ≥20 carbon atoms), methoxyphenols, and nitrophenols.

2.4 Statistical data analysis

The temporal component of organic compound groups during the sampling campaign was investigated by a clustergram for visualization of sample and variable relations using Matlab® (Version 2010b, The MathWorks, MA, USA) and its Bioinformatic Toolbox. The dendrograms, which were obtained from Ward's minimum variance algorithm and Euclidean distance applied on standardized (autoscaled) variables, illustrate the similarity of variables (i.e. chemical compound class;

rows) or observations (i.e. days; columns). The associated heatmap displays how many standard deviations a datapoint is distant from the mean. None of the included classes dropped below the limit of quantification at any sampling day, so we do not expect inflation of noise from the standardization.

A dendrogram may not accurately represent the distance matrix, which is known as ultrametric tree inequality. The cophenetic correlation coefficient denotes a metric to assess how well a dendrogram fits the distances between considered pairs of objects and is be interpreted similar to Pearson's correlation coefficient (Sokal and Rohlf, 1962).

2.5 Meteorological data and trace gas analysis

Records of the meteorological parameters including wind speed, wind direction, relative humidity (RH) and temperature (T) followed the guidelines of the Vietnamese National Technical Regulation on Meteorological Observations (MONRE, 2012). The records were done manually four times a day at midnight, 06.00 AM, noon and 06.00 PM UTC, corresponding to 07.00 AM, 01.00 PM, 07.00 PM and 01.00 AM local time. In addition, hourly averaged T and RH data were retrieved from ambient sensors at the main inlet for the aerosol and trace gas measurements. Precipitation was collected as daily bulk samples at the station. Carbon monoxide (CO), carbon dioxide (CO_2) and methane (CH_4) were measured with a cavity ring-down spectrometer (G2401; Picarro Inc., CA, USA); ozone was measured by UV absorption (Ozone Analyzer 49i; Thermo Scientific, CA, USA). The inlet height was 12 m above ground, roughly 6 m above the rooftop and about 200 m from the location of the MiniVol sampler (Bukowiecki et al., 2019).

2.6 MODIS/TERRA Fire Image and Backward Trajectory Observation Using FLEXTRA

The interpretation of the aerosol composition analyses was supported by air mass back-trajectory analysis combined with BB locations as retrieved from the Moderate Resolution Imaging Spectroradiometers (MODIS) from the Terra and Aqua platform (MODIS Collection 6 Hotspot / Active Fire Detections MCD14DL). Backward trajectories (BWT) were computed with the FLEXTRA trajectory model driven by 3-hourly meteorological analysis fields (1° x 1° resolution) of the operational Integrated Forecast System (IFS) of the European Center for Medium-range Weather Forecast (ECMWF) (Stohl, 1996;Stohl and Seibert, 1998). Trajectories were initialized every 4 hours at different heights above the site and were followed backwards in time for 10 days within the global model domain. For the discussion, trajectories started at 420 m above ground were selected, an altitude roughly in the middle between real surface and smoothed model elevation. Fire counts were aggregated for different periods of the measurement campaign and displayed as the total number of fire counts per day on a 0.25° x 0.25° grid covering the area of interest.

3 Results and discussion

3.1 Meteorology description

Figure 2 shows the time series of meteorological observations at PDI during the sampling campaign. From 23rd March to 12th April 2015, temperature ranged from 12 °C to 27°C and relative humidity between from 29% and 100% was observed. PDI received only occasionally precipitation with rainfall at the beginning and end of the sampling period. In the middle of the sampling period, hot and dry weather dominated with the highest observed temperature and lowest RH. Furthermore, the local wind direction was mostly from the West-Southwest during the dry period and Southeast during the middle of the sampling period.

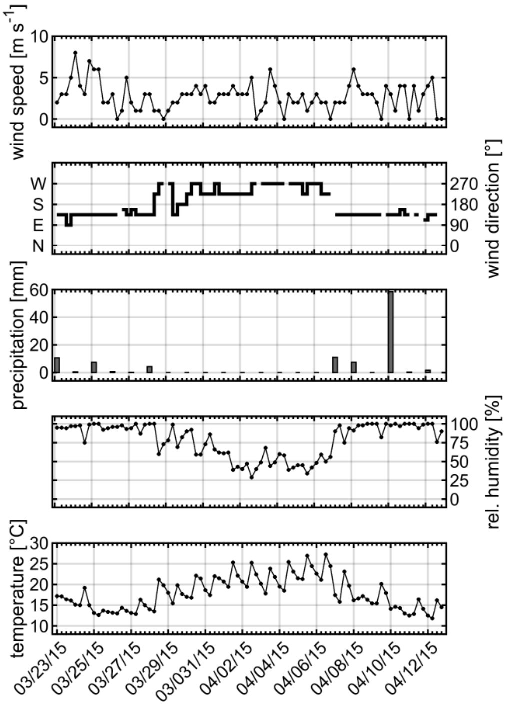

Figure 2. Time series (local time) of observed meteorological conditions at PDI during the sampling campaign from 23rd March to 12th April 2015.

3.2 PM$_{2.5}$ bulk carbonaceous component and its organic compositions

3.2.1 Organic carbon (OC), elemental carbon (EC) and levoglucosan

Figure 3a displays the temporal variations of organic carbon (OC), elemental carbon (EC) and levoglucosan concentrations determined in the daily aerosol particle samples. OC and EC concentrations span ranges of more than one order of magnitude from 1.8 to 38.3 µg m^{-3} (OC) and 0.13 to 17.8 µg m^{-3} (EC), respectively, which are comparable with those measured in the North Southeast Asia region during dry season, i.e. Sonla, Vietnam in 2012 and 2013 (OC: 1.0 – 40.6 µg m^{-3}, EC: 0.0 -7.1 µg m^{-3}, Lee et al. (2016); Phimai, central Thailand in 2006 (OC: 2.3 – 16.7 µg m^{-3}, EC: 0.0 - 6.6 µg m^{-3}, Li et al. (2013)); Suthep Mountain, Chiang Mai, Thailand in 2010 (OC: 5.1 – 26.8 µg m^{-3}, EC: 1.6 -10.4 µg m^{-3}, Chuang et al. (2013)); DoiAnKhang, Thailand in 2015 (OC: 20.0 – 75.6 µg m^{-3}, EC: 3.1 -11.1 µg m^{-3}, Pani et al. (2019a)). Highest concentrations of both OC and EC were observed on 5th and 6th April. The temporal trend of OC and EC correlated with the observed levoglucosan, which is known as a marker of BB (Simoneit et al., 1999), pointing towards substantial influence of BB on the carbonaceous aerosol content. The data are also summarized in Table S1 as average concentrations of OC, EC, and together with further constituted organics.

The ratios of OC to EC have been widely used to derive information about emission sources (Chow et al., 2004b;Han et al., 2010). Ratios of about 5 were reported in the winter in Xi-an, China, which was attributed to coal combustion for residential heating and BB; on the other hand, low ratios about 1 were attributed to vehicle and traffic-related sources. BB –influenced aerosol OC-to-EC ratios were 4.8 in Phimai, Thailand (Li et al., 2013) and ~ 6 in Chiangmai, Thailand (Chuang et al., 2013;Pani et al., 2019a), and ~ 6 in Sonla, Vietnam (Lee et al., 2016). In our study, the ratio averaged at 4.8, which is comparable with

BB-influenced aerosol in Southeast Asia. However, we emphasize that OC/EC distinctly different above one only indicates the absence of efficient combustion as dominating OC and EC source and does not permit a direct assignment to BB. We operationally defined char-EC as $EC1_{apparent}$-OP and soot-EC as EC2+EC3 according to Han et al. (2007) in order to examine the source of EC. At low concentrations of EC, soot-EC account for 50% of EC species, whereas at high EC concentrations, the fraction of char-EC increases and becomes dominant (Figure 3b). Soot-EC is considered to be more associated with motor vehicle emissions and char-EC with the combustion of solid fuels, such as biomass or coal (Han et al., 2010), indicating changing emission sources of EC and an association of high EC concentrations with solid fuel combustion during the sampling period. Furthermore, three distinct groups may be recognized from the EC species: (1) 12 days with less 2.0 µg m^{-3} of char-EC; (2) 6 days with of char-EC between 2.0 µg m^{-3} and 7.0 µg m^{-3}; and (3) two days with more than 7.0 µg m^{-3} of char-EC. Since char-EC and levoglucosan are highly correlated (Pearson's r of 0.96), we derive that during the sampling campaign there were three periods with varying degrees of BB influence on $PM_{2.5}$ composition.

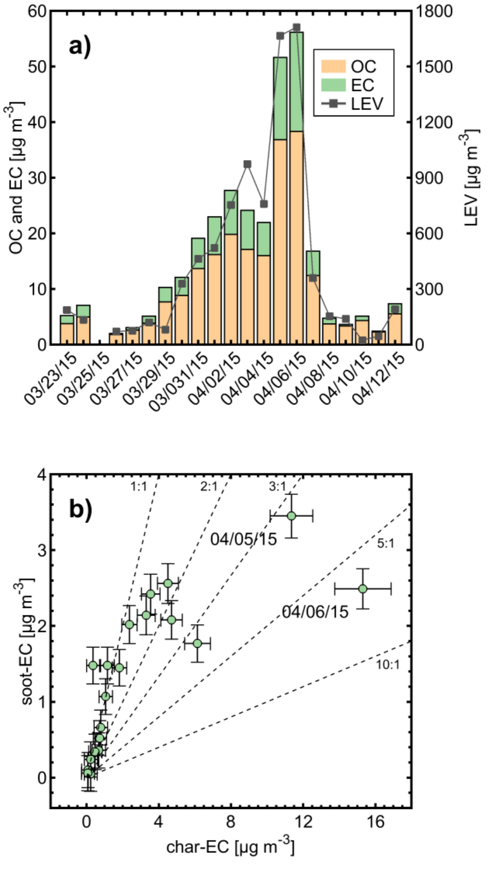

Figure 3. a) Temporal variations of OC, EC and levoglucosan (LEV) as BB marker in $PM_{2.5}$ at PDI during the sampling campaign from 23rd March to 12th April 2015; **b)** Scatterplot of char-EC vs soot-EC during sampling campaign. Error bars represent measurement uncertainty calculated with formula (1) with precision and LOD of 10% and 0.36 µg m^{-3} for char-EC and 5% and 0.23 µg m^{-3} for soot-EC, respectively. Dashed lines indicate the ratio of char-EC to soot-EC.

3.2.2 Cluster analysis of Organic Aerosol Composition

We grouped the data from chemical OA speciation into the classes PAH, o-PAH, anhydrous sugars, methoxyphenols, nitrophenols, fatty acids, and n-alkanes and performed together with OC a hierarchical cluster analysis in order to examine if the broadly defined OA composition follows the same trend as OC, EC and levoglucosan. A clustergram (Figure **4**) was used to illustrate days and classes related to organic particle constituents with similar composition and temporal behavior, respectively. A clustergram consists of a heatmap in the center with two dendrograms in horizontal and vertical position, generally illustrating similarities of variables and observations. The dendrogram of the upper part of the clustergram suggests three major time periods with distinctly different OA composition. Based on the previous section, we label the days "low BB-influence", "medium BB-influence", and "high BB-influence". The dendrogram on the left hand side emphasizes which variables are best representing the classification of the days and give insights why individual days stick out within one of the three major clusters. For both dendrograms in the clustergram, the cophenetic correlation coefficient is >0.95, showing excellent representation of the pairwise distances within variables and within observation. It can be derived that the BB-related compound classes of methoxy-phenols and anhydrosugars seem to originate from the same source and to a lesser extent fatty acids and alkanes. Since OC, PAHs and OPAH do not follow the same trend as the methoxyphenols and anhydrous sugars, we can expect significant contribution from other sources, such as traffic or in the case of elevated levels of o-PAH and OC, atmospheric ageing. Nitrophenols show a different temporal behavior, thus appearing on an isolated branch of the dendrogram. Of all considered compound classes, nitrophenols on 5th April had the largest absolute distance of 4.1σ from the campaign mean. We keep the classification of the sampling days by the clustergram for further discussion of the data in the following sections.

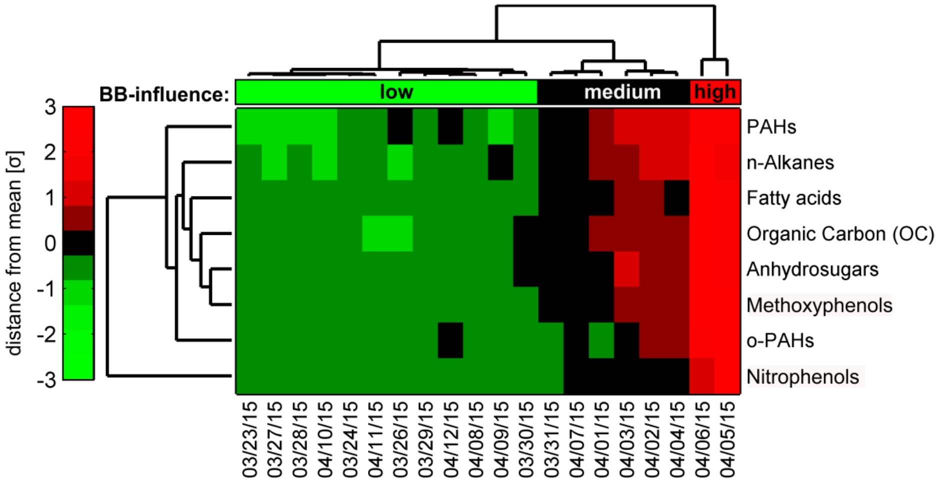

Figure 4. Clustergram based on organic composition of $PM_{2.5}$ sampled at PDI during the sampling campaign from 23rd March to 12th April 2015. Dendrograms indicating organic compounds and OC can be seen at the top and sampling days clustering on the left of the diagram. The colorbar on the left indicates the shades associated with values in the cells and denotes the distance to the mean in multiples of the standard deviation σ: Dark to bright green denotes the lower values, dark to bright red the higher values and black refers to values closest to the mean.

3.2.3 Molecular composition of aerosol constituents

In this section, molecular constituents of OA and their possible origins are discussed compound class-wise and presented in Figure 5. Additional information is provided in the Supplement Figure S1 and Figure S2. In total, the quantified OA constituents account for up to 4% of OC.

3.2.3.1 Anhydrosugars

Anhydrosugars, including levoglucosan, mannosan and galactosan, produced by pyrolysis of cellulose and hemicellulose, are universal markers for BB (Simoneit and Elias, 2001). Levoglucosan is the most abundant organic compound in OC (23 – 1710 ng m^{-3}, 0.22 – 2.5% of OC), and increased with increasing OC concentrations, indicating a significant impact of BB at receptor site. Ratios of levoglucosan to mannosan may give an indication of the type of biomass. However, due to high levoglucosan deposit on the filter samples, broad peaks in IDTD-GCMS analysis partially overlapped with mannosan and galactosan, which led to high uncertainty of the quantitative results for the latter components. Hence, we omit to discuss ratios of individual anhydrous sugar species except levoglucosan, but used mannosan and galactosan together with levoglucosan in total concentrations of anhydrosugars. Additional determination of the isotopic ratios in anhydrosugars would allow a more specific identification of the BB source, such as woody biomass or crop residues (Sang et al., 2012).

3.2.3.2 Methoxyphenols

Methoxyphenols are products from the pyrolysis of biomass containing lignin, a constituent of all vascular plants present mostly between cellular structures and cell walls, and admit to differentiate between angiosperms, gymnosperms and gramineae (Simoneit, 2002). Vanillin and vanillic acid are markers for conifers (gymnosperm), whereas syringaldehyde, syringic acid are released from the combustion of angiosperms (and also found minor amounts in gymnosperm smoke.), and m-/p-hydroxybenzoic acid and acetosyringone are characteristic for gramineae (referring to grasses and non-woody vegetation).

During the sampling period, m-, p-hydroxybenzoic acid and acetosyringone appeared in range of 0.8 - 247 ng m^{-3} and 0.1 - 49.0 ng m^{-3}, respectively, which may be linked to agricultural residue burning practice in the northern Southeast Asia. Syringaldehyde, and syringic acid were in the range of at 0.0 - 40.2 and 0.1 - 47.9 ng m^{-3}, respectively, whereas vanillin and vanillic acid were found in lower quantities (0.2 – 11.8 ng m^{-3}, and 0.1 – 49.1 ng m^{-3}). Based on the relative abundance of typical lignin monomers of gymnosperms, open BB smoke contributions appear to originate predominantly from burning grasses and angiosperms. Moreover, the temporal fluctuation of the relative abundances of phenolic species with one or no additional substituent at the aromatic ring indicates different types of BB during medium-BB and high-BB days.

3.2.3.3 High Molecular Weight (HMW) n-Alkanes (C20:C33)

The daily summed concentrations of targeted n-alkanes ranged from 7.2 to 262 ng m^{-3} during sampling period. The concentrations were in the range from 7.2 to 45 ng m^{-3} within days of low BB-influence and concentrations up to 262 ng m^{-3} for days with high BB influence. We calculated the Carbon Preference Index (CPI) from the relation of n-alkanes with odd and even carbon number and determined and the most abundant n-alkane for each day (C_{max}). Originally, the CPI for higher plant wax was calculated using n-alkanes from C21 to C34 (Simoneit, 1989). However, because of missing data for C34, we modified the CPI for this study by including n-alkanes from C21 to C32 to CPI_{21-32}.

The main source of n-alkanes is epicuticular plant growth showing a strong dominance of odd-numbered carbon chain lengths with a maximum concentration (C_{max}) at C_{29} and C_{31}. Another possible source of n-alkanes are vehicle emissions with a maximum abundance at C_{25} for gasoline and C_{20} for heavy duty within the range of C_{19} to C_{32} (Simoneit, 1986). Emissions from the combustion of fossil fuels have typically a CPI of about 1, while emissions of biogenic origin (e.g. plant abrasion, emissions from biomass combustion) often have a CPI of >2 (Simoneit and Mazurek, 1982).

CPI values for days with low BB influence ranged from 0.95 to 1.6, which indicated a dominating contribution of fossil carbon sources (Cohen et al., 2010) to the organic matter despite the remote location of the sampling station. On the other hand, CPI values for days with medium- and high-BB influence were from 1.5 to 2.8, inferring together with C_{max} of 29 the input from biogenic sources and suspension of debris from BB (Figure S3).

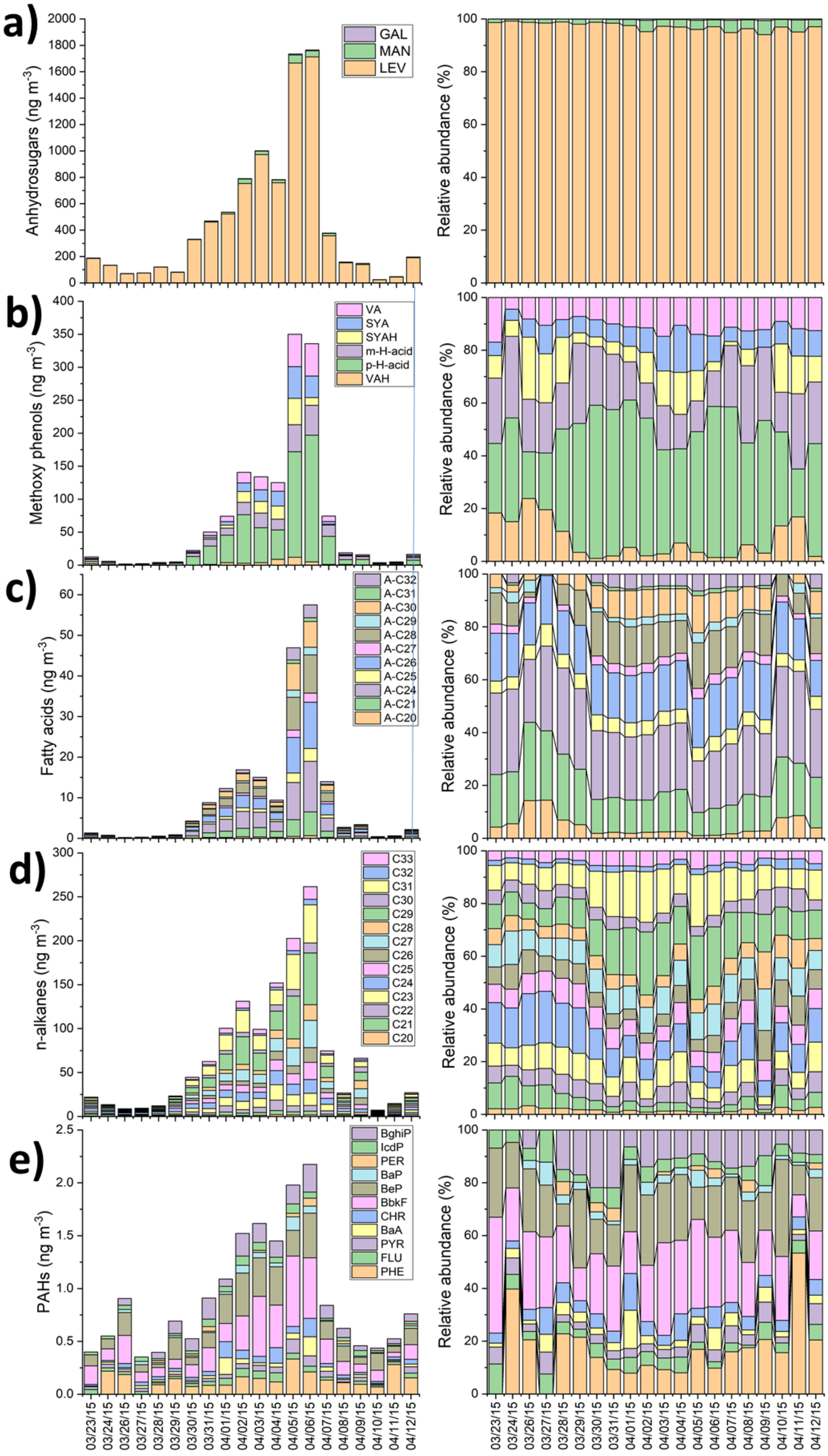
a)
Anhydrosugars (ng m^{-3})
2000
1800
1600
1400
1200
1000
800
600
400
200
0
GAL
MAN
LEV
Relative abundance (%)
100
80
60
40
20
0
b)
Methoxy phenols (ng m^{-3})
400
350
300
250
200
150
100
50
0
VA
SYA
SYAH
m-H-acid
p-H-acid
VAH
Relative abundance (%)
c)
Fatty acids (ng m^{-3})
60
50
40
30
20
10
0
A-C32
A-C31
A-C30
A-C29
A-C28
A-C27
A-C26
A-C25
A-C24
A-C21
A-C20
Relative abundance (%)
d)
n-alkanes (ng m^{-3})
300
250
200
150
100
50
0
C33
C32
C31
C30
C29
C28
C27
C26
C25
C24
C23
C22
C21
C20
Relative abundance (%)
e)
PAHs (ng m^{-3})
2.5
2.0
1.5
1.0
0.5
0.0
BghiP
IcdP
PER
BaP
BeP
BbkF
CHR
BaA
PYR
FLU
PHE
Relative abundance (%)
03/23/15
03/24/15
03/26/15
03/27/15
03/28/15
03/29/15
03/30/15
03/31/15
04/01/15
04/02/15
04/03/15
04/04/15
04/05/15
04/06/15
04/07/15
04/08/15
04/09/15
04/10/15
04/11/15
04/12/15

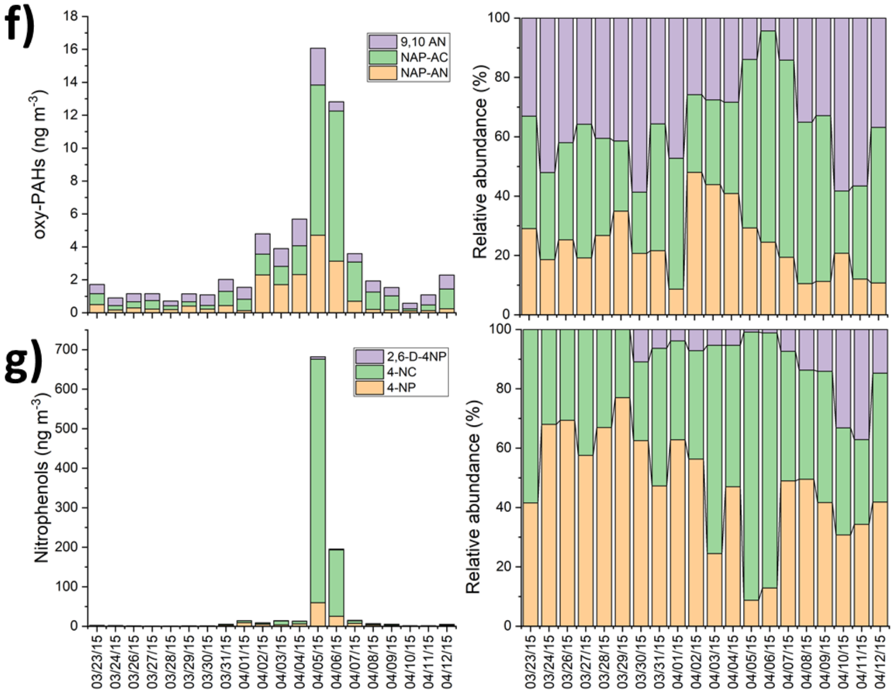

Figure 5. Time series of organic constituents in daily aerosol particle samples (n=21) at PDI during the sampling campaign from 23rd March to 12th April 2015. a) anhydrosugars, b) methoxyphenols, c) n-fatty acids, d) n-alkanes, e) PAHs, f) o-PAHs, g) nitrophenols. Left column provides mass concentrations (µg m^{-3}) and right column provides relative mass fractions within the compound class.

3.2.3.4 High Molecular Weight (HMW) Fatty Acids (C20:C32)

HMW fatty acids are released from terrestrial higher plant waxes, but also from different kinds of BB, cooking and vehicular emissions (Ren et al., 2020). During BB events, lipid-related compounds that are originally present as leaf-waxes can be emitted to the air together with smoke particles via volatilization, absorption, and trapped onto particulate matter without oxidative degradation. Enhancement of HMW fatty acids concentration coincided with levoglucosan and HMW n-alkanes during intensive wheat straw burning periods in Mt. Tai, northern China and Nanjing, East China (Wang et al., 2009;Fu et al., 2012). The daily summed concentrations of HMW fatty acids were ranged from 0.2 – 57.5 ng m^{-3} during sampling period, in which the low range (0.2 – 3.4 ng m^{-3}) of concentration took place at the beginning and at the end of sampling period, belonging to low-BB days. HMW fatty acids with even carbon number showed higher concentrations than the ones with odd carbon number, pointing toward domination of biogenic origin.

3.2.3.5 PAHs

The following eleven PAHs, which are known as markers for incomplete combustion, were quantified: phenanthrene (PHE), fluoranthene (FLU), pyrene (PYR), benz[a]anthracene (BaA), chrysene (CHR), sum of benzo[b]fluoranthene and benzo[k]fluoranthene (BbkF), benz[e]pyrene (BeP), benz[a]pyrene (BaP), perylene (PER), indeno[1,2,3-cd]pyrene (IcdP), and benzo[ghi]perylene (BghiP). The sum concentrations of detected PAHs cover the range of 0.35 – 2.17 ng m^{-3} and 0.26 - 1.95 ng m^{-3} without considering PHE, respectively, which is sensitive to sampling conditions because of its volatility. Among the targeted PAHs, PER showed the lowest average concentration (range: 0.00 – 0.07 ng m^{-3}), while the BbkF showed the highest average concertation (range: 0.04 – 0.67 ng m^{-3}). All individual PAHs reached their highest concentrations during the 05th and 06th April with high suspected influence of BB (Figure 5). Comparing total PAHs in the vicinity of the study area, the resolved PAHs were much lower concentrated than those found in the BacGiang and HaNam, rural sites in north of Vietnam (80 - 2200, and 170 – 800 ng m^{-3} respectively) (Anh et al., 2019), but comparable with those found in Chiangmai, Thailand in dry season (0.3 – 6.8 ng m^{-3}) (Chuesaard et al., 2013).

The ratio of some selected PAHs can be useful to roughly discriminate PAH sources. Such PAH diagnostic ratios account for different formation mechanisms in combustion or atmospheric degradation and are available for a wide range of sources, e.g. stationary coal, oil, natural gas and wood combustion as well as cooking emissions and vehicle exhaust emissions (Tobiszewski and Namiesnik, 2012). Petrogenic PAH are predominantly abundant in fossil carbon sources and emitted as unburned fuel or in leakages of fuel storage, whereas pyrogenic PAH are formed by pyrolysis at high temperatures (Abdel-Shafy and Mansour, 2016). During the entire campaign, there was a noticeable influence of pyrogenic PAH to ambient PM2.5, indicated by the median diagnostic ratio of 0.62. However, neither the diagnostic ratios for combustion sources follow the trends of molecular markers for BB, such as levoglucosan or lignin monomers, nor they show elevated values for the high-BB days (Figure 6 left). Moreover, in the diagnostic ratio consisting of BeP and BaP, the faster degradation of BaP in the atmosphere is exploited with values below 0.5 indicating degradation of the aerosol by photochemical aging (Tobiszewski and Namiesnik, 2012). However, the BaP/(BaP+BeP) is unknown for the fresh emission and recent studies revealed that BaP/(BaP+BeP) for residential heating (Miersch et al., 2019;Vicente et al., 2016) may fall below the threshold of 0.5. Apart from three days, all BaP/(BaP+BeP) were below 0.15, pointing toward atmospheric aging. The maximum of 0.35 appeared on 5th April, which belongs to one of the two high-BB days and coincides with the maximum observed concentrations of nitrophenols discussed in section 3.2.3.7.

Altogether, PAH diagnostic ratios and PAH pattern are not useful in this data set to elucidate their emission sources and could not linked to BB, which agrees with the relatively large distance of PAH to BB markers such as anhydrous sugars and methoxyphenols. Major differences in PAH patterns arise from semi-volatile three- and four-ring PAH PHE, FLU and PYR, which may be caused by dynamic gas-particle partitioning. The classification of the days rather corresponds to the total concentrations of PAH, which were found to be significantly different ($p < 0.05$) between low-, medium- and high BB periods using a one-way analysis of variance (ANOVA) with Bonferroni post-hoc correction.

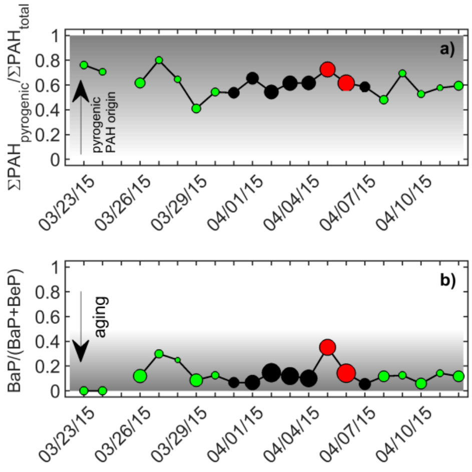

Figure 6. PAH diagnostic ratios to estimate a) the contribution pyrogenic PAH and b) influence of atmospheric aging. Colors denote the previously defined periods with low (green), medium (black) and high (red) influence of BB. Dot sizes represent a relative metric for the total concentration of PAH involved in the respective diagnostic ratio.

3.2.3.6 Oxygenated PAH (o-PAHs)

Three o-PAHs have been quantified and are discussed in this study: 9,10-Anthracenedione (9,10-AN), 1,8-naphthalic anhydride (NAP-AN), naphthoic acid (NAP-AC). o-PAHs are associated with incomplete gasoline, diesel, coal or wood combustion as well as with the photo oxidation of the PAH precursors (Walgraeve et al., 2010). The total concentrations of the three o-PAHs varied between 0.19 ng m^{-3} and 5.36 ng m^{-3}, peaking during the high-BB days 5th and 6th April. Among the o-PAHs, 9,10-AN showed the lowest average concentration (0.75 ng m^{-3}), while NAP-AC showed the highest average concertation (1.62 ng m^{-3}). It seems that 9,10-AN is less associated with the observed BB plume due to its relatively low concentration range and distinct lower relative contribution to total o-PAH concentrations during high-BB days. At the beginning of the medium-BB period, NAP-AN had its highest relative abundance during the sampling campaign and declined on the following days while NAP-AC steadily increased, which moderately correlates with the ambient temperature (Figure 2). In the aqueous phase, NAP-AN may be rapidly hydrolyzed to NAP-AC depending on the temperature and pH (Barros et al., 2001). Therefore, only the sum of NAP-AN and NAP-AC should be used for source apportionment.

3.2.3.7 Nitrophenols

Nitrophenols may originate from various primary sources, e.g. traffic, coal and biomass combustion, herbicide and pesticide usage, but are predominantly formed by reactions of mono-aromatic compounds with OH radicals and NO$_x$ (Harrison et al., 2005;Li et al., 2016;Kahnt et al., 2013). An important subclass of nitrophenols are nitrocatechols which belong to the group of are UV-light-absorbing species (Brown Carbon) and are known to affect the radiative balance and climate of Earth (Laskin et al., 2015).

The compounds 4-nitrophenol (4-NP) and 4-nitrocatechol (4-NC) account for 0.4-60.0 ng m^{-3} and 0.2 -616.0 ng m^{-3}, respectively. Typically, peak concentrations coincided with enhanced levoglucosan abundance on 5th and 6th April, and reached enhancement factors up to 10 (4-NP) and 600 (4-NC) compared to other low and medium BB-influenced days during sampling campaign. 4-NP in our study was lower than that of in haze episode in Shanghai (range 150- 770 ng m^{-3}), but much higher than in one-year study in Belgium (range 0.32 - 1.03). In contrast, 4-NC in our study was higher than that of in Shanghai (22 – 154 770 ng m^{-3}) and in Belgium (0.49 - 9.0 ng m^{-3}). This might be explained by short atmospheric aging of the BB plume prior to arrival since nitrophenols are rapidly formed from monoaromatics by photooxidation as well as reaction with nitrate radicals. Because of 24 h filter sampling, day and nighttime chemistry as well as sampling artifacts cannot be unambiguously distinguished. However, it has been reported that the formation of 4-NC from catechol proceeds approximately three times faster during night than during daytime (Finewax et al., 2018). Hence, substantially elevated levels of nitrophenols may be a result of atmospheric aerosol transport during nighttime.

3.3. Trace gases observations and implications

Figure **6** 7 shows the time series of hourly averaged CO, O$_3$, CO$_2$ and CH$_4$ mixing ratios during the sampling campaign. The temporal evolution of these records also indicates the different conditions that were observed during the campaign.

CO mixing ratios were in the range of 220 – 600 ppb at the beginning and the end of the sampling campaign, but increased slowly from late March before reaching up to 1270 ppb on 5th April. Each year from February to May, CO levels at PDI are systematically enhanced and do not represent background mixing ratios as expected to be observed at a pristine sampling site. The latter is the case from June to September when CO mixing ratios below 100 ppb are often observed (see also Bukowiecki et al. (2019)). The enhancement in spring can be explained by the widespread open BB in Southeast Asia (Lin et al., 2013) and particularly all over the Indochina peninsula in spring (Yen et al., 2013), which leads to high emissions of CO (Shi and Yamaguchi, 2014;Lelieveld et al., 2001). The observed variability and the additional increase by more than 800 ppb of CO during specific days of the campaign confirms the hypothesis of advection of more regional BB events (Kondo et al., 2004;Pochanart et al., 2003).

https://doi.org/10.5194/acp-2020-1027
Preprint. Discussion started: 28 October 2020

After rainfall on 07th April, CO dropped back to the range observed before, but still did not reach typical values for the unpolluted boundary layer. O_3 shows a similar pattern like CO: mixing ratios had rather small variability in the beginning before they increased to up to 90 ppb, followed by a sharp drop to only 4 ppb. CO_2 and CH_4 also show increases in their mixing ratios on 5th and 6th April, but with less variability. However, unlike CO and O_3, the mixing ratios of CO_2 and CH_4 remained elevated also after the BB event and the following rainfall likely due to the north-easterly advection of anthropogenic emissions (see the trajectory analysis below).

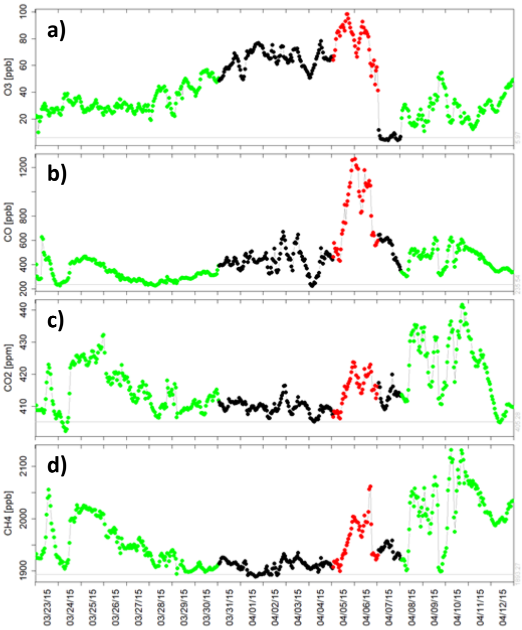

Figure 7. Time series of hourly a) ozone (O_3), b) carbon monoxide (CO), c) carbon dioxide (CO_2) and d) methane (CH_4) at PDI during the sampling campaign from 23rd March to 12th April 2015. Three colors, including green, black, and red follow the clustergram from statistical approach discussed in section 3.3. Grey lines in the plots indicate the background values, calculated as the mean of the lowest 5% of the dataset during the campaign.

Scatterplots of hourly averaged trace gases indicate different relationships between these gases during the sampling campaign (Figure 8.). The correlation between CO vs CH_4 reveals two apparent branches, the upper (in red) was observed on 5th and 6th April when BB influence was high, the lower (in green) in the beginning and the end of the campaign. The distinction of the different BB influence regimes is best seen in the scatter plots with CO, which reflects the large contribution of BB to the atmospheric CO burden, especially during the high BB influence days. Therefore, the gas trace observations confirm the classification of the sampling days based on the chemical composition of $PM_{2.5}$ in the clustergram.

Correlations of CO_2, CH_4 and CO with O_3 are less evident due to the above mentioned different sources, formation and removal processes. Nevertheless, the excess $\Delta O_3/\Delta CO$ ratio is a commonly used proxy to investigate the age of BB plumes (Jaffe and Wigder, 2012) and to characterize O_3 production in smoke plumes. In general, $\Delta O_3/\Delta CO$ usually increases with increasing plume age of the BB plume due to net O_3 production (Parrington et al., 2013;Akagi et al., 2011;Jaffe and Wigder, 2012). ΔO_3 and ΔCO were calculated by subtracting the "baseline" during the campaign which was determined as the average of the lowermost 5% of the data during the campaign (see the grey lines in Figure 7). However, reported values for the $\Delta O_3/\Delta CO$ ratio in aged plumes do not show a consistent pattern (between 0.1 and 0.9, Figure S4) for some plumes associated with tropical fires (Andreae et al., 1994;Mauzerall et al., 1998) and boreal fires (Honrath et al., 2004;Bertschi and Jaffe, 2005) and as low as 0.1 in aged plumes from Southeast Asian studies (Kondo et al., 2004) as ozone formation also depends on the availability of nitrogen oxides and volatile organic compounds. To account for BB influence, we linked $\Delta O_3/\Delta CO$ ratios with levoglucosan during sampling campaign. During days with low BB influence, levoglucosan concentrations were in the range of 20-400 ng m^{-3} and the $\Delta O_3/\Delta CO$ ratio increased from 0.05 to 0.8 (see Fig. S3), indicating other source contributions for O_3 production, i.e. photochemical conversion of biogenic VOC emissions (Nguyen et al., 2016). During days with medium BB influence, levoglucosan levels increased up to 1000 ng m^{-3}, and the excess ratio slightly decreased while being more variable. On 5th and 6th April with high BB influence, levoglucosan concentrations reached up to 1.6 µgm^{-3} and the excess ratio dropped below 0.1 especially on 6th of April, suggesting that the arriving BB plume was rather fresh. Right after the high BB plume event, $\Delta O_3/\Delta CO$ does not allow unambiguous interpretation because O_3 levelled off close to the background. The last part of the campaign, identified to be under low BB influence, is characterized by mostly low $\Delta O_3/\Delta CO$ ratios, which only tend to increase towards the end of the campaign. It must be also emphasized that the calculation of the excess ratios is sensitive to the selection of the background levels, increasing uncertainty for $\Delta O_3/\Delta CO$.

The MCE (modified combustion efficiency: $\Delta CO_2/(\Delta CO+\Delta CO_2)$) was widely used as an indicator of combustion emissions, with higher MCE values (close to 1) indicating higher proportions of flaming/complete combustion and lower MCEs referring to higher proportions of smoldering/incomplete combustion (Kondo et al., 2011). In particular, MCE was observed in the ranges from 0.80 to 1.00 for wildland fires in several vegetation zones (Akagi et al., 2011) and 0.79 to 0.98 in regional smoke plume at the Mount Bachelor Observatory (Briggs et al., 2016). MCE was stable around 0.98 from the beginning of the period and decreased to values below 0.94 from 30th March to 4th April. It reached lowest values below 0.9 on 05th April, while it rises again back to 0.99 afterwards (see Fig. S3). Variability in MCE was found particularly between 30th March and 6th April, which might be caused by variable degrees of mixing between the smoke plume and other air masses (Yokelson et al., 2013). As for the $\Delta O_3/\Delta CO$, both CO and CO_2 are close to the chosen background. Consequently, at CO_2 mixing ratios below 410 ppm, the uncertainty of MCE exceeds 0.04.

We examined the relation between MCE and the compound classes defined in Figure 3. Concentrations of all compound classes declined with increasing MCE due to more efficient combustion conditions (Figure S5). The absolute values of the slopes are similar to the intercepts obtain from the regression (Table S1), giving reasonable concentrations of organic close to detection of ideal combustion with MCE of 1. PAHs and -alkanes, which cannot be formed by atmospheric aging, show the best agreement with the regression function, whereas the fit for nitrophenols is clearly dominated by the datapoints of the high-BB days, indicating formation by secondary processes.

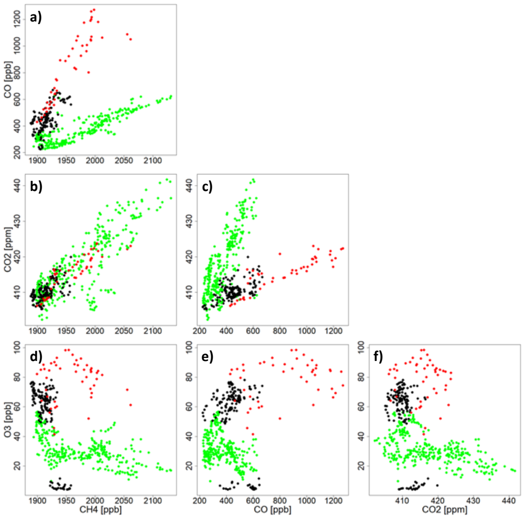

Figure 8. Scatter plots of hourly ozone (O_3), carbon monoxide (CO), carbon dioxide (CO_2) and methane (CH_4) vs. each other at PDI during the sampling campaign from 23rd March to 12th April 2015. Three colors, including green, black, and red follow the clusters of low-, medium-, and high-influenced BB discussed in section 3.2.2.

3.4. Back trajectory analysis

Average air mass backward trajectories for each of the periods identified by the organic aerosol clustering reveal a distinctly different advection pattern for the 3 pollution phases (Figure 9). Similar plots of individual trajectories (initialized on a 4-hourly time step) can be found in the supplemental material (Figure S6). For the low pollution phase, atmospheric transport towards PDI was from north-eastern to eastern sector with a stronger tendency of trajectories arriving from mainland China after the polluted phase (April) as compared arriving over the Yellow sea before the polluted phase (March). Very little active BB was observed by MODIS in these regions. In clear contrast, air mass trajectories indicate the arrival of air from the south-western sector during the pollution event passing directly over large areas of active open BB in northern Laos (most intense) and Myanmar (less intense) (Pani et al., 2019b;Lin et al., 2013). A main difference between the more polluted cluster (high) and the medium polluted cluster (medium) seems to be a recirculation over land area for the medium cluster as compared to a more westerly advection for the high cluster. On average air masses moved slightly faster in the high-BB cluster (larger distance between symbols in trajectory plot) than in the medium cluster. However, in both cases the area with the most intense fires was crossed within the last 24 to 36 hours before arriving at PDI, supporting the finding of little aging in the aerosol composition as derived from $\Delta O_3/\Delta CO$. Fire activities were more enhanced during the high-BB days than medium-BB days (see Figure S4), potentially explaining the observed differences in pollution loads. For all OA clusters, the average trajectories were travelling below 2 km above sea level in the last five days before arrival at PDI, suggesting that sampled air masses were in immediate contact with surface emissions.

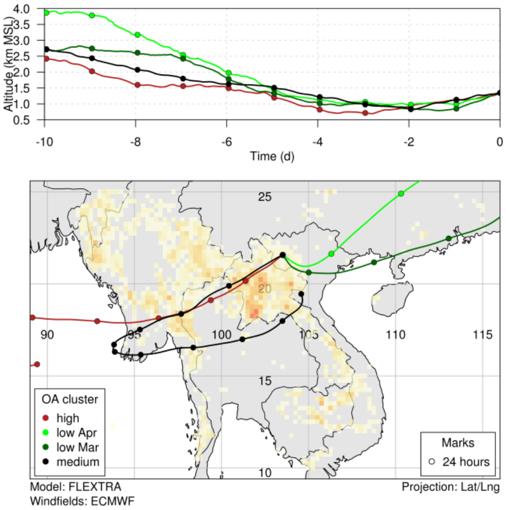

Figure 9. Ten-day backward trajectories arriving at PDI averaged for the periods determined by the organic aerosol clustering. The "low" class was additionally split into the period before the BB event (March: low Mar) and after (April: low Apr). The upper panel displays the average height of the trajectories above sea level on a relative time axis before arrival at the site. The lower panel gives the average location of the trajectories overlaid on a map of MODIS fire count densities for the period spanning from five days before until the end of the investigation period (from low (bright yellow) to high (orange-red) fire intensities). Filled circles on the trajectories mark a travel time of 24 hours.

4. Conclusions

Our comprehensive characterization of carbonaceous $PM_{2.5}$ species and monitoring of trace gases at the Pha Din (PDI) station in Vietnam from 23rd March to 12th April 2015 gives insights into aerosol composition during the pre-monsoon season. OC and EC concentrations in $PM_{2.5}$ were found in the range from 1.8 to 38.3 µg m^{-3} and 0.1 to 9.8 µg m^{-3}, and comparable with other studies in the region during the dry season. Among several organic compound classes and 51 quantified OA constituents, anhydrous sugars and levoglucosan were the most abundant compound class and species, respectively. In a combined statistical and molecular marker approach, together with trace gases and BWT analysis, a consistent picture could be drawn that there were three distinct pollution periods with elevated levels of organic aerosol loadings associated with BB aerosol of different kinds, such as wildfires or the combustion of post-harvest agricultural residues. The analyses of BWT, fire counts and $\Delta O_3/\Delta CO$ point toward a short plume age of less than 36 hours for the air masses of high-BB influence days and local/regional BB events by implication. However, daily averaged MCE > 0.90 remained high compared to literature values of BB plumes. Furthermore, enhanced concentrations of nitrophenols on 5th and 6th April indicate that short atmospheric aging changed the chemical composition and thus the properties of BB aerosol. In contrast, the ratios of OC to EC of these two days (2.2 and 2.5) are equal/less than the first quartile (2.5) of the entire sampling period; thus we cannot detect any formation of secondary OC, either caused by absence of secondary OC formation or by missing data points for primary OC and EC.

Overall, our results agree with a previous source apportionment study based on optical aerosol properties (Bukowiecki et al., 2019), and add valuable data on the OC chemical composition of $PM_{2.5}$ in a region of scarce data availability.

Acknowledgement

This work was financially supported via research grant No.91614707 by German Academic Exchange Service (DAAD) and No. QTRU05.01/18-20 by Vietnam Academy of Science and Technology (VAST). HC thanks for funding by the Helmholtz International Lab *aeroHEALTH* (InterLabs-0005) through the Federal German Helmholtz Association of Research Centers (HGF) and the Helmholtz Zentrum München. The continuous aerosol optical property and trace gas observations were setup and operated with support of the Federal Office of Meteorology and Climatology MeteoSwiss through the project Capacity Building and Twinning for Climate Observing Systems (CATCOS) Phase 1 and Phase 2, Contract No. 81025332 between the Swiss Agency for Development and Cooperation (SDC) and MeteoSwiss. We thank the Vietnam Meteorological and Hydrological Administration (VNMHA) for providing access to the facilities and for the support of our measurements. MS acknowledges funding from the GAW Quality Assurance/Science Activity Centre Switzerland (QA/SAC-CH) which is supported by MeteoSwiss and Empa. OBP thanks to Russian Fond for Basic Research (RFBR), grant No. 20-55-12001. We acknowledge the use of data and imagery from LANCE FIRMS operated by NASA's Earth Science Data and Information System (ESDIS) with funding provided by NASA Headquarters.

Author contributions

Experimental work at the sampling site was done by DLN. DLN performed IDTD-GC-TOF-MS and thermal-optical carbon analyses with assistance from JO and GA. DLN, HC and JSK analyzed IDTD-GC-TOF-MS and TOR data; HC conducted the statistical analysis of IDTD-GC-TOFMS data; MS and DLN performed the trace gas data analyses; SH conducted the back trajectory analysis. Data interpretation was done by DLN, HC, SMP, MS, SH, OBP and JSK. HC, JSK, GE and XAN supervised the study. XAN, DLN, OBP and JSK acquired the funding. The manuscript was written by DLN, HC and SMP with contribution from all authors.

Data and code availability

The continuous trace gas records from Pha Din are available on the dedicated GAW data repositories, i.e. O_3 data can be found at the World Data Centre for Reactive Gases (www.gaw-wdcrg.org), while CO_2, CH_4, and CO data are available on the World Data Centre for Greenhouse Gases (https://gaw.kishou.go.jp/). The trajectory model FLEXTRA is open source software that can be obtained from www.flexpart.eu. Trajectory plots for the site PDI can be inspected at the following link: https://lagrange.empa.ch/FLEXTRA_browser/data_access.php?stat=PDI&year=2015&prod=_hourly_. Further data is available from the corresponding author upon request.

References

Abdel-Shafy, H. I., and Mansour, M. S.: A review on polycyclic aromatic hydrocarbons: source, environmental impact, effect on human health and remediation, Egyptian journal of petroleum, 25, 107-123, 2016.

Akagi, S., Yokelson, R. J., Wiedinmyer, C., Alvarado, M., Reid, J., Karl, T., Crounse, J., and Wennberg, P.: Emission factors for open and domestic biomass burning for use in atmospheric models, Atmos Chem Phys, 11, 4039, 2011.

Andreae, M., Anderson, B., Blake, D., Bradshaw, J., Collins, J., Gregory, G., Sachse, G., and Shipham, M.: Influence of plumes from biomass burning on atmospheric chemistry over the equatorial and tropical South Atlantic during CITE 3, Journal of Geophysical Research: Atmospheres, 99, 12793-12808, 1994.

Anh, H. Q., Minh, T. B., Tran, T. M., and Takahashi, S.: Road dust contamination by polycyclic aromatic hydrocarbons and their methylated derivatives in northern Vietnam: concentrations, profiles, emission sources, and risk assessment, Environmental Pollution, 254, 113073, 2019.

Barros, T. C., Yunes, S., Menegon, G., Nome, F., Chaimovich, H., Politi, M. J., Dias, L. G., and Cuccovia, I. M.: Hydrolysis of 1, 8-and 2, 3-naphthalic anhydrides and the mechanism of cyclization of 1, 8-naphthalic acid in aqueous solutions, Journal of the Chemical Society, Perkin Transactions 2, 2342-2350, 2001.

Bertschi, I. T., and Jaffe, D. A.: Long-range transport of ozone, carbon monoxide, and aerosols to the NE Pacific troposphere during the summer of 2003: Observations of smoke plumes from Asian boreal fires, Journal of Geophysical Research: Atmospheres, 110, 2005.

Briggs, N. L., Jaffe, D. A., Gao, H., Hee, J. R., Baylon, P. M., Zhang, Q., Zhou, S., Collier, S. C., Sampson, P. D., and Cary, R. A.: Particulate matter, ozone, and nitrogen species in aged wildfire plumes observed at the Mount Bachelor Observatory, Aerosol and Air Quality Research, 16, 2016.

Bruns, E., El Haddad, I., Keller, A., Klein, F., Kumar, N., Pieber, S., Corbin, J., Slowik, J., Brune, W., and Baltensperger, U.: Inter-comparison of laboratory smog chamber and flow reactor systems on organic aerosol yield and composition, Atmospheric Measurement Techniques, 8, 2315-2332, 2015.

Bukowiecki, N., Steinbacher, M., Henne, S., Nguyen, N. A., Nguyen, X. A., Hoang, A. L., Nguyen, D. L., Duong, H. L., Engling, G., Wehrle, G., Gysel-Beer, M., and Baltensperger, U.: Effect of Large-scale Biomass Burning on Aerosol Optical Properties at the GAW Regional Station Pha Din, Vietnam, Aerosol and Air Quality Research, 19, 1172-1187, 10.4209/aaqr.2018.11.0406, 2019.

Carmichael, G. R., Tang, Y., Kurata, G., Uno, I., Streets, D., Woo, J. H., Huang, H., Yienger, J., Lefer, B., Shetter, R., Blake, D., Atlas, E., Fried, A., Apel, E., Eisele, F., Cantrell, C., Avery, M., Barrick, J., Sachse, G., Brune, W., Sandholm, S., Kondo, Y., Singh, H., Talbot, R., Bandy, A., Thorton, D., Clarke, A., and Heikes, B.: Regional-scale chemical transport modeling in support of the analysis of observations obtained during the TRACE-P experiment, Journal of Geophysical Research: Atmospheres, 108, 10.1029/2002jd003117, 2003.

Chan, C. Y., L. Y. Chan, J. M. Harris, S. J. Oltmans, D. R. Blake, Y. Qin, Y. G. Zheng, and X. D. Zheng: Characteristics of biomass burning emission sources, transport, and chemical speciation in enhanced springtime tropospheric ozone profile over Hong Kong, Journal of Geophysical Research: Atmospheres, 108, 10.1029/2001jd001555, 2003.

Chow, J. C., Watson, J. G., Chen, L. W., Arnott, W. P., Moosmuller, H., and Fung, K.: Equivalence of elemental carbon by thermal/optical reflectance and transmittance with different temperature protocols, Environ Sci Technol, 38, 4414-4422, 10.1021/es034936u, 2004a.

Chow, J. C., Watson, J. G., Kuhns, H., Etyemezian, V., Lowenthal, D. H., Crow, D., Kohl, S. D., Engelbrecht, J. P., and Green, M. C.: Source profiles for industrial, mobile, and area sources in the Big Bend Regional Aerosol Visibility and Observational study, Chemosphere, 54, 185-208, 10.1016/j.chemosphere.2003.07.004, 2004b.

Chuang, M.-T., Chou, C. C. K., Sopajaree, K., Lin, N.-H., Wang, J.-L., Sheu, G.-R., Chang, Y.-J., and Lee, C.-T.: Characterization of aerosol chemical properties from near-source biomass burning in the northern Indochina during 7-SEAS/Dongsha experiment, Atmos Environ, 78, 72-81, 10.1016/j.atmosenv.2012.06.056, 2013.

Chuesaard, T., Chetiyanukornkul, T., Kameda, T., Hayakawa, K., and Toriba, A.: Influence of biomass burning on the levels of atmospheric polycyclic aromatic hydrocarbons and their nitro derivatives in Chiang Mai, Thailand, Aerosol Air Quality Research, 14, 1247-1257, 2013.

Cohen, D. D., Crawford, J., Stelcer, E., and Bac, V. T.: Long range transport of fine particle windblown soils and coal fired power station emissions into Hanoi between 2001 to 2008, Atmos Environ, 44, 3761-3769, 10.1016/j.atmosenv.2010.06.047, 2010.

Engling, G., Zhang, Y.-N., Chan, C.-Y., Sang, X.-F., Lin, M., Ho, K.-F., Li, Y.-S., Lin, C.-Y., and Lee, J. J.: Characterization and sources of aerosol particles over the southeastern Tibetan Plateau during the Southeast Asia biomass-burning season, Tellus B: Chemical and Physical Meteorology, 63, 117-128, 10.1111/j.1600-0889.2010.00512.x, 2011.

Finewax, Z., de Gouw, J. A., and Ziemann, P. J.: Identification and Quantification of 4-Nitrocatechol Formed from OH and NO3 Radical-Initiated Reactions of Catechol in Air in the Presence of NO x: Implications for Secondary Organic Aerosol Formation from Biomass Burning, Environ Sci Technol, 52, 1981-1989, 2018.

Fu, P. Q., Kawamura, K., Chen, J., Li, J., Sun, Y. L., Liu, Y., Tachibana, E., Aggarwal, S. G., Okuzawa, K., Tanimoto, H., Kanaya, Y., and Wang, Z. F.: Diurnal variations of organic molecular tracers and stable carbon isotopic composition in atmospheric aerosols over Mt. Tai in the North China Plain: an influence of biomass burning, Atmos Chem Phys, 12, 8359-8375, 10.5194/acp-12-8359-2012, 2012.

Gautam, R., Hsu, N. C., Eck, T. F., Holben, B. N., Janjai, S., Jantarach, T., Tsay, S.-C., and Lau, W. K.: Characterization of aerosols over the Indochina peninsula from satellite-surface observations during biomass burning pre-monsoon season, Atmos Environ, 78, 51-59, 10.1016/j.atmosenv.2012.05.038, 2013.

Gilmour, M. I., Kim, Y. H., and Hays, M. D.: Comparative chemistry and toxicity of diesel and biomass combustion emissions, Analytical and bioanalytical chemistry, 407, 5869-5875, 10.1007/s00216-015-8797-9, 2015.

Han, Y., Cao, J., Chow, J. C., Watson, J. G., An, Z., Jin, Z., Fung, K., and Liu, S.: Evaluation of the thermal/optical reflectance method for discrimination between char-and soot-EC, Chemosphere, 69, 569-574, 2007.

Han, Y. M., Cao, J. J., Lee, S. C., Ho, K. F., and An, Z. S.: Different characteristics of char and soot in the atmosphere and their ratio as an indicator for source identification in Xi'an, China, Atmos Chem Phys, 10, 595-607, 10.5194/acp-10-595-2010, 2010.

Harrison, M. A., Barra, S., Borghesi, D., Vione, D., Arsene, C., and Olariu, R. I.: Nitrated phenols in the atmosphere: a review, Atmos Environ, 39, 231-248, 2005.

Honrath, R., Owen, R. C., Val Martin, M., Reid, J., Lapina, K., Fialho, P., Dziobak, M. P., Kleissl, J., and Westphal, D.: Regional and hemispheric impacts of anthropogenic and biomass burning emissions on summertime CO and O3 in the North Atlantic lower free troposphere, Journal of Geophysical Research: Atmospheres, 109, 2004.

Ihalainen, M., Tiitta, P., Czech, H., Yli-Pirilä, P., Hartikainen, A., Kortelainen, M., Tissari, J., Stengel, B., Sklorz, M., and Suhonen, H.: A novel high-volume Photochemical Emission Aging flow tube Reactor (PEAR), Aerosol Sci Tech, 53, 276-294, 2019.

Ihantola, T., Di Bucchianico, S., Happo, M., Ihalainen, M., Uski, O., Bauer, S., Kuuspalo, K., Sippula, O., Tissari, J., and Oeder, S.: Influence of wood species on toxicity of log-wood stove combustion aerosols: a parallel animal and air-liquid interface cell exposure study on spruce and pine smoke, Particle fibre toxicology, 17, 1-26, 2020.

Jaffe, D. A., and Wigder, N. L.: Ozone production from wildfires: A critical review, Atmos Environ, 51, 1-10, 2012.

Kahnt, A., Behrouzi, S., Vermeylen, R., Shalamzari, M. S., Vercauteren, J., Roekens, E., Claeys, M., and Maenhaut, W.: One-year study of nitro-organic compounds and their relation to wood burning in PM10 aerosol from a rural site in Belgium, Atmos Environ, 81, 561-568, 2013.

Kanashova, T., Sippula, O., Oeder, S., Streibel, T., Passig, J., Czech, H., Kaoma, T., Sapcariu, S. C., Dilger, M., and Paur, H.-R.: Emissions from a modern log wood masonry heater and wood pellet boiler: Composition and biological impact on air-liquid interface exposed human lung cancer cells, Journal of Molecular Clinical Medicine, 1, 23-35, 2018.

Kondo, Y., Morino, Y., Takegawa, N., Koike, M., Kita, K., Miyazaki, Y., Sachse, G., Vay, S., Avery, M., and Flocke, F.: Impacts of biomass burning in Southeast Asia on ozone and reactive nitrogen over the western Pacific in spring, Journal of Geophysical Research: Atmospheres, 109, 2004.

Kondo, Y., Matsui, H., Moteki, N., Sahu, L., Takegawa, N., Kajino, M., Zhao, Y., Cubison, M., Jimenez, J., and Vay, S.: Emissions of black carbon, organic, and inorganic aerosols from biomass burning in North America and Asia in 2008, Journal of Geophysical Research: Atmospheres, 116, 2011.

Laskin, A., Laskin, J., and Nizkorodov, S. A.: Chemistry of atmospheric brown carbon, Chemical reviews, 115, 4335-4382, 2015.

Lee, C.-T., Ram, S. S., Nguyen, D. L., Chou, C. C., Chang, S.-Y., Lin, N.-H., Chang, S.-C., Hsiao, T.-C., Sheu, G.-R., and Ou-Yang, C.-F.: Aerosol chemical profile of near-source biomass burning smoke in Sonla, Vietnam during 7-SEAS campaigns in 2012 and 2013, Aerosol Air Quality Research, 16, 2603-2617, 2016.

Lelieveld, J., Crutzen, P. J., Ramanathan, V., Andreae, M. O., Brenninkmeijer, C. M., Campos, T., Cass, G. R., Dickerson, R. R., Fischer, H., de Gouw, J. A., Hansel, A., Jefferson, A., Kley, D., de Laat, A. T., Lal, S., Lawrence, M. G., Lobert, J. M., Mayol-Bracero, O. L., Mitra, A. P., Novakov, T., Oltmans, S. J., Prather, K. A., Reiner, T., Rodhe, H., Scheeren, H. A., Sikka, D., and Williams, J.: The Indian Ocean experiment: widespread air pollution from South and Southeast Asia, Science, 291, 1031-1036, 10.1126/science.1057103, 2001.

Li, C., Tsay, S.-C., Hsu, N. C., Kim, J. Y., Howell, S. G., Huebert, B. J., Ji, Q., Jeong, M.-J., Wang, S.-H., Hansell, R. A., and Bell, S. W.: Characteristics and composition of atmospheric aerosols in Phimai, central Thailand during BASE-ASIA, Atmos Environ, 78, 60-71, 10.1016/j.atmosenv.2012.04.003, 2013.

Li, X., Jiang, L., Lyu, Y., Xu, T., Yang, X., Iinuma, Y., Chen, J., and Herrmann, H.: Size distribution of particle-phase sugar and nitrophenol tracers during severe urban haze episodes in Shanghai, Atmos Environ, 145, 115-127, 2016.

Lin, N.-H., Tsay, S.-C., Maring, H. B., Yen, M.-C., Sheu, G.-R., Wang, S.-H., Chi, K. H., Chuang, M.-T., Ou-Yang, C.-F., Fu, J. S., Reid, J. S., Lee, C.-T., Wang, L.-C., Wang, J.-L., Hsu, C. N., Sayer, A. M., Holben, B. N., Chu, Y.-C., Nguyen, X. A., Sopajaree, K., Chen, S.-J., Cheng, M.-T., Tsuang, B.-J., Tsai, C.-J., Peng, C.-M., Schnell, R. C., Conway, T., Chang, C.-T., Lin, K.-S., Tsai, Y. I., Lee, W.-J., Chang, S.-C., Liu, J.-J., Chiang, W.-L., Huang, S.-J., Lin, T.-H., and Liu, G.-R.: An overview of regional experiments on biomass burning aerosols and related pollutants in Southeast Asia: From BASE-ASIA and the Dongsha Experiment to 7-SEAS, Atmos Environ, 78, 1-19, 10.1016/j.atmosenv.2013.04.066, 2013.

Martinsson, J., Eriksson, A. C., Nielsen, I. E., Malmborg, V. B., Ahlberg, E., Andersen, C., Lindgren, R., Nystrom, R., Nordin, E. Z., Brune, W. H., Svenningsson, B., Swietlicki, E., Boman, C., and Pagels, J. H.: Impacts of Combustion Conditions and Photochemical Processing on the Light Absorption of Biomass Combustion Aerosol, Environment Science & Technology, 49, 14663-14671, 10.1021/acs.est.5b03205, 2015.

Mauzerall, D. L., Logan, J. A., Jacob, D. J., Anderson, B. E., Blake, D. R., Bradshaw, J. D., Heikes, B., Sachse, G. W., Singh, H., and Talbot, B.: Photochemistry in biomass burning plumes and implications for tropospheric ozone over the tropical South Atlantic, Journal of Geophysical Research: Atmospheres (1984–2012), 103, 8401-8423, 1998.

Miersch, T., Czech, H., Hartikainen, A., Ihalainen, M., Orasche, J., Abbaszade, G., Tissari, J., Streibel, T., Jokiniemi, J., and Sippula, O.: Impact of photochemical ageing on Polycyclic Aromatic Hydrocarbons (PAH) and oxygenated PAH (Oxy-PAH/OH-PAH) in logwood stove emissions, Science of the total environment, 686, 382-392, 2019.

MONRE: National Technical Regulation on meterological Observations - QCVN 46 : 2012/BTNMT, Vietnam National Technical Regulations, 2012.

Nguyen, D. L., Kawamura, K., Ono, K., Ram, S. S., Engling, G., Lee, C.-T., Lin, N.-H., Chang, S.-C., Chuang, M.-T., and Hsiao, T.-C.: Comprehensive PM2. 5 organic molecular composition and stable carbon isotope ratios at Sonla, Vietnam: Fingerprint of biomass burning components, Aerosol and Air Quality Research, 16, 2618-2634, 2016.

Nordin, E. Z., Uski, O., Nyström, R., Jalava, P., Eriksson, A. C., Genberg, J., Roldin, P., Bergvall, C., Westerholm, R., and Jokiniemi, J.: Influence of ozone initiated processing on the toxicity of aerosol particles from small scale wood combustion, Atmos Environ, 102, 282-289, 2015.

Orasche, J., Schnelle-Kreis, J., Abbaszade, G., and Zimmermann, R.: In-situ derivatization thermal desorption GC-TOFMS for direct analysis of particle-bound non-polar and polar organic species, Atmos Chem Phys, 11, 8977-8993, 2011.

Pani, S. K., Chantara, S., Khamkaew, C., Lee, C.-T., and Lin, N.-H.: Biomass burning in the northern peninsular Southeast Asia: Aerosol chemical profile and potential exposure, Atmospheric Research, 224, 180-195, 2019a.

Pani, S. K., Ou-Yang, C.-F., Wang, S.-H., Ogren, J. A., Sheridan, P. J., Sheu, G.-R., and Lin, N.-H. J. A. E.: Relationship between long-range transported atmospheric black carbon and carbon monoxide at a high-altitude background station in East Asia, Atmos Environ, 210, 86-99, 2019b.

Pardo, M., Li, C., He, Q., Levin-Zaidman, S., Tsoory, M., Yu, Q., Wang, X., and Rudich, Y.: Mechanisms of lung toxicity induced by biomass burning aerosols, Particle fibre toxicology, 17, 4, 2020.

Parrington, M., Palmer, P., Lewis, A., Lee, J., Rickard, A., Di Carlo, P., Taylor, J., Hopkins, J., Punjabi, S., and Oram, D.: Ozone photochemistry in boreal biomass burning plumes, Atmos Chem Phys, 13, 7321-7341, 2013.

Pham, C. T., Boongla, Y., Nghiem, T. D., Le, H. T., Tang, N., Toriba, A., and Hayakawa, K.: Emission Characteristics of Polycyclic Aromatic Hydrocarbons and Nitro-Polycyclic Aromatic Hydrocarbons from Open Burning of Rice Straw in the North of Vietnam, International journal of environmental research and public health, 16, 2343, 10.3390/ijerph16132343, 2019.

Pochanart, P., Akimoto, H., Kajii, Y., and Sukasem, P.: Carbon monoxide, regional-scale transport, and biomass burning in tropical continental Southeast Asia: Observations in rural Thailand, Journal of Geophysical Research: Atmospheres, 108, 2003.

Popovicheva, O. B., Engling, G., Diapouli, E., Saraga, D., Persiantseva, N. M., Timofeev, M., Kireeva, E. D., Shonija, N. K., Chen, S.-H., and Nguyen, D. L.: Impact of smoke intensity on size-resolved aerosol composition and microstructure during the biomass burning season in Northwest Vietnam, Aerosol Air Quality Research, 16, 2635-2654, 2016.

Popovicheva, O. B., Shonija, N. K., Persiantseva, N., Timofeev, M., Diapouli, E., Eleftheriadis, K., Borgese, L., and Nguyen, X. A.: Aerosol pollutants during agricultural biomass burning: A case study in Ba Vi region in Hanoi, Vietnam, Aerosol Air Quality Research, 17, 2762-2779, 2017.

Reid, J. S., Hyer, E. J., Johnson, R. S., Holben, B. N., Yokelson, R. J., Zhang, J., Campbell, J. R., Christopher, S. A., Di Girolamo, L., and Giglio, L.: Observing and understanding the Southeast Asian aerosol system by remote sensing: An initial review and analysis for the Seven Southeast Asian Studies (7SEAS) program, Atmospheric Research, 122, 403-468, 2013.

Ren, L., Zhou, T., and Zhang, W.: Attribution of the record-breaking heat event over Northeast Asia in summer 2018: the role of circulation, Environmental Research Letters, 15, 054018, 2020.

Sang, X. F., Gensch, I., Laumer, W., Kammer, B., Chan, C. Y., Engling, G., Wahner, A., Wissel, H., Kiendler-Scharr, A. J. E. s., and technology: Stable carbon isotope ratio analysis of anhydrosugars in biomass burning aerosol particles from source samples, 46, 3312-3318, 2012.

Seinfeld, J. H., and Pandis, S. N.: Atmospheric chemistry and physics: from air pollution to climate change, John Wiley & Sons, 2016.

Shi, Y., and Yamaguchi, Y.: A high-resolution and multi-year emissions inventory for biomass burning in Southeast Asia during 2001–2010, Atmos Environ, 98, 8-16, 2014.

Simoneit, B. R., and Mazurek, M. A.: Organic matter of the troposphere—II. Natural background of biogenic lipid matter in aerosols over the rural western United States, Atmospheric Environment (1967), 16, 2139-2159, 1982.

Simoneit, B. R.: Characterization of organic constituents in aerosols in relation to their rigin and transport: a review, International Journal of Environmental Analytical Chemistry, 23, 207-237, 1986.

Simoneit, B. R.: Organic matter of the troposphere—V: application of molecular marker analysis to biogenic emissions into the troposphere for source reconciliations, Journal of Atmospheric Chemistry, 8, 251-275, 1989.

Simoneit, B. R., and Elias, V. O.: Detecting organic tracers from biomass burning in the atmosphere, Marine Pollution Bulletin, 42, 805-810, 10.1016/s0025-326x(01)00094-7, 2001.

Simoneit, B. R. T., Schauer, J. J., Nolte, C. G., Oros, D. R., Elias, V. O., Fraser, M. P., Rogge, W. F., and Cass, G. R.: Levoglucosan, a tracer for cellulose in biomass burning and atmospheric particles, Atmos Environ, 33, 173-182, 10.1016/s1352-2310(98)00145-9, 1999.

Simoneit, B. R. T.: Biomass burning — a review of organic tracers for smoke from incomplete combustion, Appl Geochem, 17, 129-162, 10.1016/s0883-2927(01)00061-0, 2002.

Sokal, R. R., and Rohlf, F. J.: The comparison of dendrograms by objective methods, Taxon, 33-40, 1962.

Stohl, A.: Trajectory statistics-a new method to establish source-receptor relationships of air pollutants and its application to the transport of particulate sulfate in Europe, Atmos Environ, 30, 579-587, 1996.

Stohl, A., and Seibert, P.: Accuracy of trajectories as determined from the conservation of meteorological tracers, Quarterly Journal of the Royal Meteorological Society, 124, 1465-1484, 1998.

Streets, D. G., Yarber, K. F., Woo, J. H., and Carmichael, G. R.: Biomass burning in Asia: Annual and seasonal estimates and atmospheric emissions, Global Biogeochem Cy, 17, n/a-n/a, 10.1029/2003gb002040, 2003.

Tobiszewski, M., and Namiesnik, J.: PAH diagnostic ratios for the identification of pollution emission sources, Environmental Pollution, 162, 110-119, 10.1016/j.envpol.2011.10.025, 2012.

Tsay, S.-C., Maring, H. B., Lin, N.-H., Buntoung, S., Chantara, S., Chuang, H.-C., Wiriya, W., Yen, M.-C., Pani, S. K., Pantina, P., Sayer, A. M., Tao, W.-K., Wang, S.-H., Welton, E. J., Lau, W. K. M., Lee, C.-T., Lee, J., Loftus, A. M., Nguyen, A. X., Nguyen, C. M., Gabriel, P. M., Goodloe, C. S., Holben, B. N., Hsiao, T.-C., Hsu, N. C., and Janjai, S.: Satellite-Surface Perspectives of Air Quality and Aerosol-Cloud Effects on the Environment: An Overview of 7-SEAS/BASELInE, Aerosol and Air Quality Research, 16, 2581-2602, 10.4209/aaqr.2016.08.0350, 2016.

Vicente, E. D., Vicente, A. M., Bandowe, B. A. M., and Alves, C. A.: Particulate phase emission of parent polycyclic aromatic hydrocarbons (PAHs) and their derivatives (alkyl-PAHs, oxygenated-PAHs, azaarenes and nitrated PAHs) from manually and automatically fired combustion appliances, Air Quality, Atmosphere & Health, 9, 653-668, 2016.

Walgraeve, C., Demeestere, K., Dewulf, J., Zimmermann, R., and Van Langenhove, H.: Oxygenated polycyclic aromatic hydrocarbons in atmospheric particulate matter: Molecular characterization and occurrence, Atmos Environ, 44, 1831-1846, 2010.

Wang, G., Kawamura, K., Xie, M., Hu, S., Cao, J., An, Z., Waston, J. G., and Chow, J. C.: Organic molecular compositions and size distributions of chinese summer and autumn aerosols from nanjing: characteristic haze event caused by wheat straw burning, Environment Science & Technology, 43, 6493-6499, 10.1021/es803086g, 2009.

Yen, M.-C., Peng, C.-M., Chen, T.-C., Chen, C.-S., Lin, N.-H., Tzeng, R.-Y., Lee, Y.-A., and Lin, C.-C.: Climate and weather characteristics in association with the active fires in northern Southeast Asia and spring air pollution in Taiwan during 2010 7-SEAS/Dongsha Experiment, Atmos Environ, 78, 35-50, 10.1016/j.atmosenv.2012.11.015, 2013.

Yokelson, R. J., Andreae, M. O., and Akagi, S.: Pitfalls with the use of enhancement ratios or normalized excess mixing ratios measured in plumes to characterize pollution sources and aging, Atmospheric Measurement Techniques, 6, 2155, 2013.

Zhong, M., and Jang, M.: Dynamic light absorption of biomass-burning organic carbon photochemically aged under natural sunlight, Atmos Chem Phys, 14, 2014.